

Supporting Information

Molecular-Level Proximity of Metal and Acid Sites in MFI Zeolite-Encapsulated Pt Nanoparticles for Selective Multistep Tandem Catalysis

Hong Je Cho,[†] Doyoung Kim,[†] Shuang Li,[‡] Dong Su,[‡] Ding Ma,[§] and Bingjun Xu^{†,*}

[†]Department of Chemical and Biomolecular Engineering, University of Delaware, Newark, Delaware 19716, United States

[‡]Center for Functional Nanomaterials, Brookhaven National Laboratory, Upton, New York 11973, United States

[§]College of Chemistry and Molecular Engineering, Peking University, Beijing 100871, China

*Correspondence: bxu@udel.edu

Materials Synthesis

Synthesis of H-ZSM-5 with different particle sizes

H-ZSM-5 samples with different particle sizes were hydrothermally synthesized, according to earlier literature.¹ Typically, tetraethylorthosilicate (TEOS, 99%, Alfa Aesar), deionized water and TPAOH (40 wt%, Alfa Aesar) were mixed, followed by stirring at 60 °C for 24 h. To this mixture, aluminum nitrate nonahydrate ($\text{Al}(\text{NO}_3)_3 \cdot 9\text{H}_2\text{O}$, 98%, Sigma Aldrich) and NaOH were added at room temperature. The molar composition of the prepared gel was 1 SiO_2 /0.25 TPAOH/0.0083 Al_2O_3 /0.05 Na_2O /8.3-100 H_2O . Thereafter, the gel was crystallized at 180 °C for 24 h. Na-ZSM-5 samples were obtained by calcination of the as-crystallized samples in air at 550 °C for 12 h. The calcined Na-ZSM-5 samples were ion-exchanged with 1 M aqueous solution of NH_4NO_3 (99%, Sigma Aldrich) at 80 °C for 2 h. This process was repeated three times. The H-ZSM-5 samples were obtained by calcination at 550 °C for 8 h.

As a result, when the prepared gel had the molar composition of H_2O of 8.3, 40 and 100, the average particle size of the corresponding H-ZSM-5 zeolites was 100 nm, 300 nm and 700 nm, respectively. The resultant samples are referred to as H-ZSM-5-100nm, H-ZSM-5-300nm and H-ZSM-5-700nm, respectively.

Synthesis of H-Al-SPP (self-pillared pentasil) zeolite

H-Al-SPP was synthesized, following the method reported in earlier literature.² In a typical synthesis, aluminium isopropoxide (Sigma Aldrich) and tetraethyl orthosilicate (TEOS, 99%, Alfa Aesar) were mixed under stirring. To this mixture, tetrabutylphosphonium hydroxide solution (TBPOH, 40 wt%, Sigma Aldrich) was added dropwise under stirring. Afterwards, NaOH (Fischer Scientific) and deionized water were mixed with the solution under stirring. After stirring for 24 h, a clear sol with composition 1 SiO_2 /0.3 TBPOH/0.005 Al_2O_3 /0.0125 Na_2O /10 H_2O was transferred into a Teflon-lined stainless steel autoclave, and heated for 14 days in an oven at 125 °C. After crystallization, Na-Al-SPP was obtained by washing with deionized water, drying at 80 °C overnight and calcination in air at 550 °C for 12 h. In order to convert Na-Al-SPP into H-Al-SPP, Na-Al-SPP was ion-exchanged with 1 M aqueous solution of NH_4NO_3 (99%, Sigma Aldrich) at 80 °C for 2 h. This process was repeated three times. H-Al-SPP was obtained from calcination at 550 °C for 8 h.

Catalyst Evaluation

Catalyst evaluation for oxidation reactions of cyclohexanol (Cy6-ol) and cyclododecanol (Cy12-ol)

To quantify the encapsulation degree of Pt NPs of Pt@H-ZSM-5, size-selective oxidation of Cy6-ol and Cy12-ol was employed, according to earlier literature.³ In 8 mL glass vial (Fisher Scientific), 0.1 mmol of Cy6-ol or Cy12-ol, 0.3 mmol of *tert*-butyl hydroperoxide (TBHP, 5.0–6.0 M in decane, Sigma Aldrich) and catalysts were mixed with 2 mL acetonitrile. The reactions over Pt@H-ZSM-5 and Pt/SiO₂ catalysts were carried out at 60 °C for 2 h under stirring. Next, turnover frequency (TOF) was calculated when a product yield was below ~10%. The ratio between TOFs for Cy6-ol and Cy12-ol ($X_{\text{sample}} = \text{TOF}_{\text{Cy6-ol}} / \text{TOF}_{\text{Cy12-ol}}$) is used as a measure of the extent to which Pt NPs are encapsulated in zeolite matrices.⁴ The encapsulation degree of Pt NPs (Z_{sample}) are defined as $Z_{\text{sample}} = 1 - 1/Y_{\text{sample}}$ where $Y_{\text{sample}} = X_{\text{sample}}/X_{\text{Pt/SiO}_2}$.⁴

Product quantification

After reactions, reaction mixtures were filtered, and then analyzed by an FID detector on GC (Agilent 7890B GC) with a CP-Volamine column. The products were identified using the standard reference compounds.

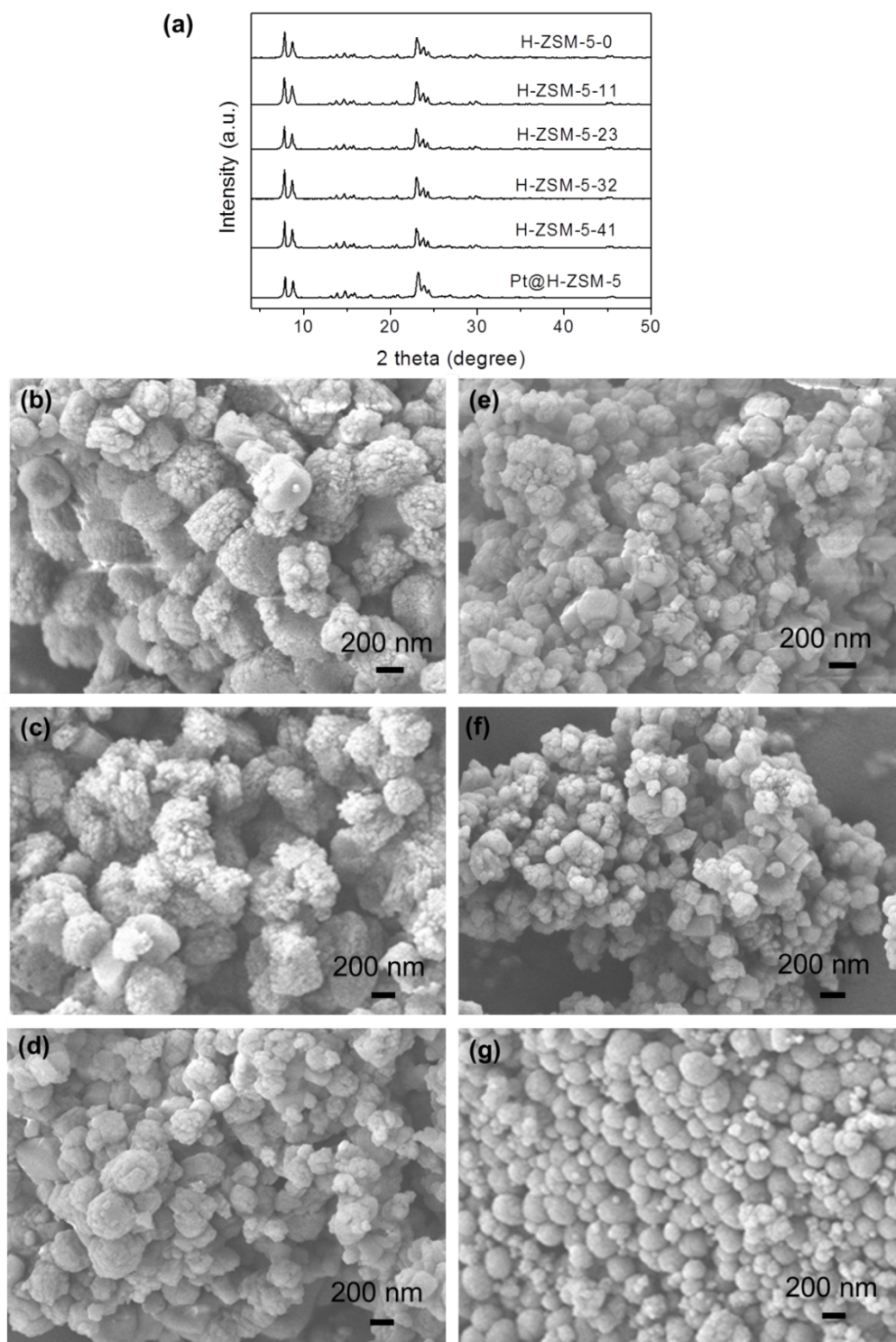


Figure S1. (a) XRD patterns of H-ZSM-5-X samples and Pt@H-ZSM-5, and SEM images of (b) Pt@H-ZSM-5, (c) H-ZSM-5-41, (d) H-ZSM-5-32, (e) H-ZSM-5-23, (f) H-ZSM-5-11 and (g) H-ZSM-5-0.

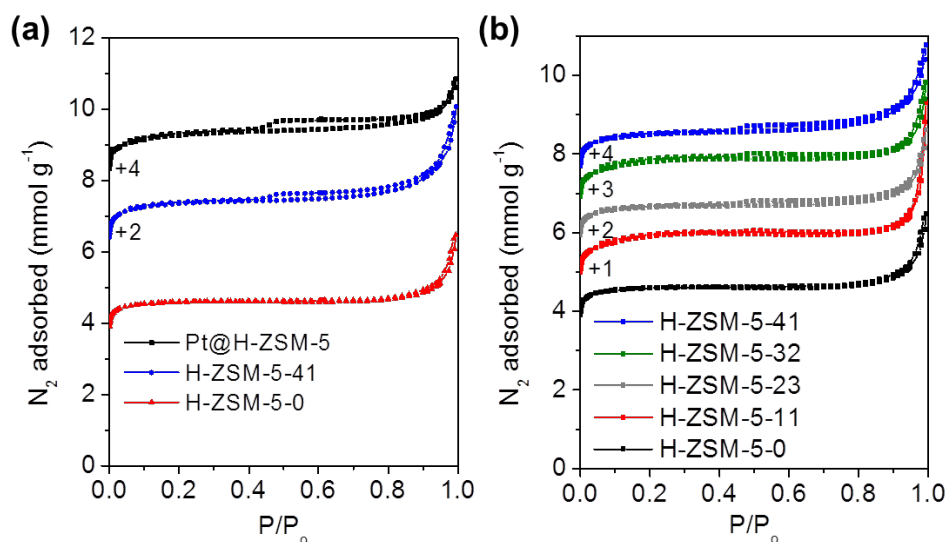


Figure S2. N₂ physisorption isotherms of (a) Pt@H-ZSM-5, H-ZSM-5-41 and H-ZSM-5-0, and (b) H-ZSM-5-*X* samples with *X* = 0-41.

Note: A step increase at relative pressure (P/P_0) < 0.05 in the isotherms signifies the presence of microporosity of zeolites. Micropore volumes of all samples are determined to be 0.14-0.15 cm³ g⁻¹ by the *t*-plot method (Table S1), which are typical for the MFI topology.^{5,6} The sharp nitrogen uptake at $P/P_0 > 0.8$ could be attributed to the intercrystalline space among the agglomerates, regardless of whether PDDA is used in the synthesis (Figure S1).

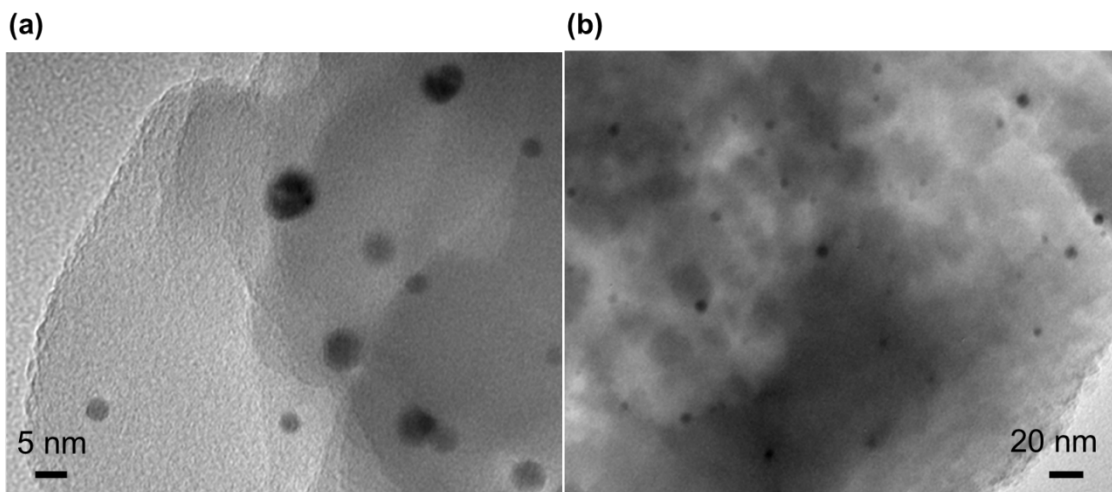


Figure S3. TEM images of Pt@H-ZSM-5 at (a) high and (b) low magnifications.

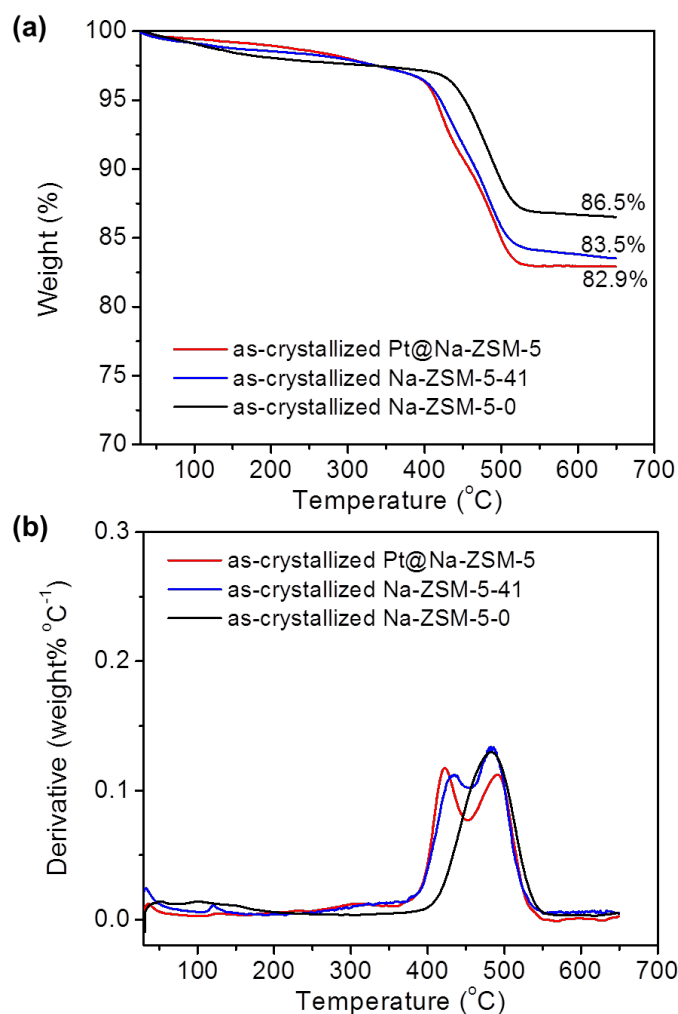


Figure S4. (a) Thermogravimetric analysis (TGA) curves and (b) their derivative (DTA) curves of the as-crystallized Pt@Na-ZSM-5, Na-ZSM-5-41 and Na-ZSM-5-0.

Note: TGA curves of the as-crystallized Pt@Na-ZSM-5, Na-ZSM-5-41 and Na-ZSM-5-0 confirm that PDDA is occluded in the as-crystallized Pt@Na-ZSM-5 and Na-ZSM-5-41 samples. Weight loss of 17.1% and 16.5% is observed on the as-crystallized Pt@Na-ZSM-5 and Na-ZSM-5-41, respectively, which are significantly higher than that of the as-crystallized Na-ZSM-5-0 (13.5%). Derivative of TGA (DTA) curves of the as-crystallized Pt@Na-ZSM-5 and Na-ZSM-5-41 indicate the weight loss likely occurring in three steps. Water is desorbed from the solid below 170 °C, and the regions of 170-430 °C and 430-550 °C are assigned to the decomposition of PDDA and TPA, respectively. These assignments are consistent with results from the as-crystallized ZSM-5-0, on which the only one high temperature weight loss peak at 400-550 °C is observed in DTA due to the lack of PDDA in its synthesis. Thus, TGA and DTA results indicate that the PDDA polymers are occluded in the samples prepared by the use of the polymers. Subsequent removal of the PDDA and TPA during calcination allows for the formation of dual micro- and meso-porosity in Pt@H(Na)-ZSM-5 as well as the hierarchical zeolites.

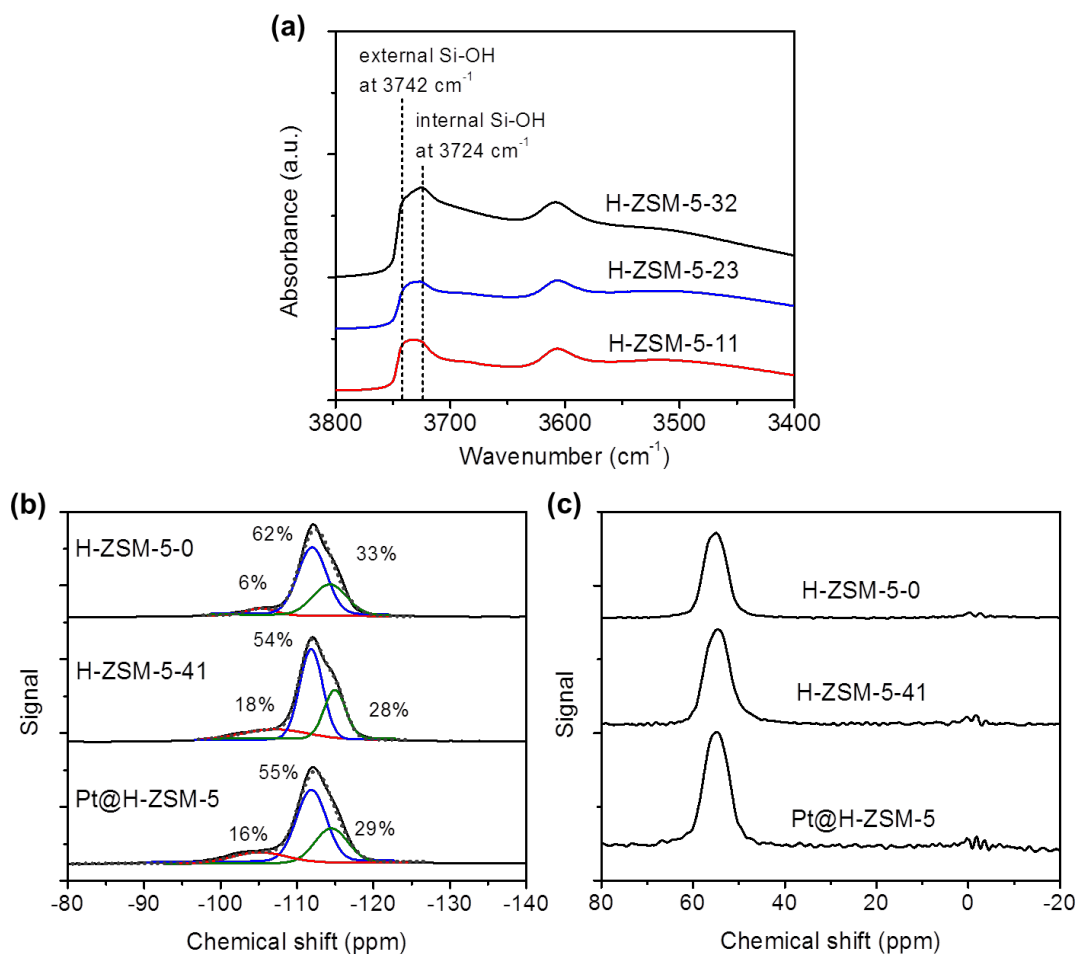


Figure S5. FTIR spectra in OH stretch range; (a) H-ZSM-5-32, 23 and 11 samples, and the spectra of (b) ²⁹Si MAS NMR and (c) ²⁷Al MAS NMR of H-ZSM-5-0, H-ZSM-5-41 and Pt@H-ZSM-5.

Note: ²⁹Si MAS NMR spectra show that Pt@H-ZSM-5 has similar framework Si structures to H-ZSM-5-41, both of which are quite distinct from H-ZSM-5-0 (Figure S5b). The two bands at -115 ppm and -111 ppm correspond to Q⁴ Si(0Al), while the chemical shift at -105 ppm corresponds to Q³ Si(1Al) or SiOH(OSi)₃.^{7, 8} The key difference between the two samples with PDDA in the synthesis (H-ZSM-5-41 and Pt@H-ZSM-5) and the one that does not (H-ZSM-5-0) is the significantly larger fraction of the Q³ peak from the former two (16%-18%) than the latter (6%). After accounting for the differences in the Si/Al ratio of the three samples (Pt@H-ZSM-5 (Si/Al = 57), H-ZSM-5-41 (Si/Al = 57) and H-ZSM-5-0 (Si/Al = 46) measured by XRF (Table S2), the SiOH(OSi)₃ fraction is determined to be 14.3%, 16.3% and 3.9% for Pt@H-ZSM-5, H-ZSM-5-41 and H-ZSM-5-0, respectively. Thus, the density of Si-OH groups on Pt@H-ZSM-5 and H-ZSM-5-41 is roughly four times as much as that on H-ZSM-5-0. ²⁷Al MAS NMR spectra of Pt@H-ZSM-5, H-ZSM-5-41 and H-ZSM-5-0 show a strong peak centered at 55 ppm associated with tetrahedrally coordinated Al in zeolite framework and a weak peak at 0 ppm (Figure S5c) corresponding to extra-framework Al sites.^{7, 9, 10} This finding indicates that the majority of Al atoms are incorporated in the MFI framework.

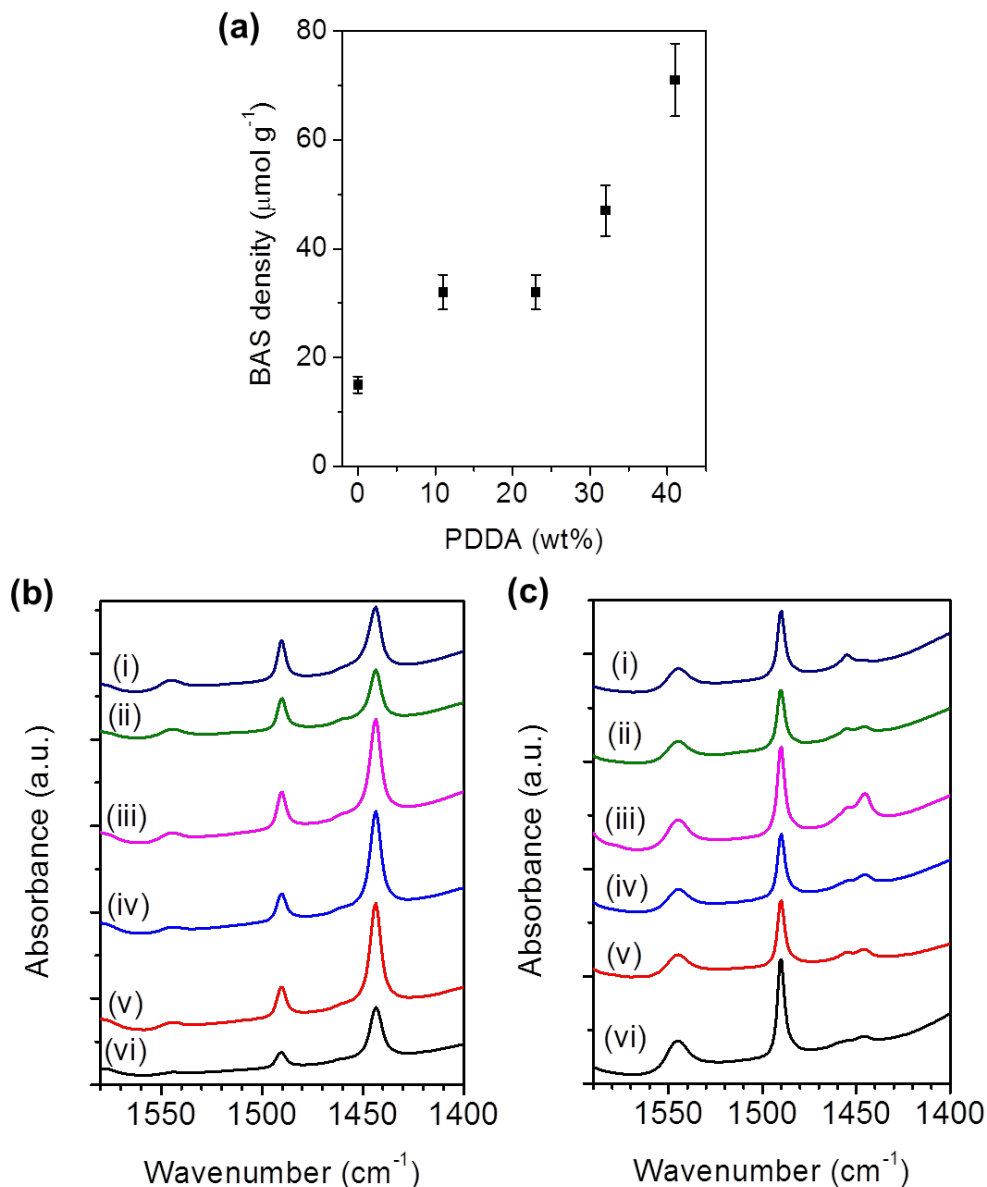


Figure S6. (a) BAS density of Na-ZSM-5-X samples as a function of the amount of PDDA used in the synthesis. FTIR spectra of samples before (b) and after (c) ion exchange with NH_4NO_3 saturated with pyridine at $150\text{ }^\circ\text{C}$. Traces in (b) are (i) Pt@Na-ZSM-5, (ii) Na-ZSM-5-41, (iii) Na-ZSM-5-32, (iv) Na-ZSM-5-23, (v) Na-ZSM-5-11 and (vi) Na-ZSM-5-0, and traces in (c) are (i) Pt@H-ZSM-5, (ii) H-ZSM-5-41, (iii) H-ZSM-5-32, (iv) H-ZSM-5-23, (v) H-ZSM-5-11 and (vi) H-ZSM-5-0. BAS densities in (a) are determined by quantitative FTIR spectroscopy with pyridine as the probe molecule at $150\text{ }^\circ\text{C}$, and are tabulated in Table S2.

Note: Na-ZSM-5-0 has BAS density of $15\text{ }\mu\text{mol g}^{-1}$ (Figure S6a). The presence of BAS on Na-ZSM-5-0 is attributed to a small fraction of the framework negative charge ($\text{Si-O}^-\text{-Al}$) balanced by tetrapropylammonium (TPA^+) used as an OSDA during zeolite crystallization, which then turns into BAS upon calcination.

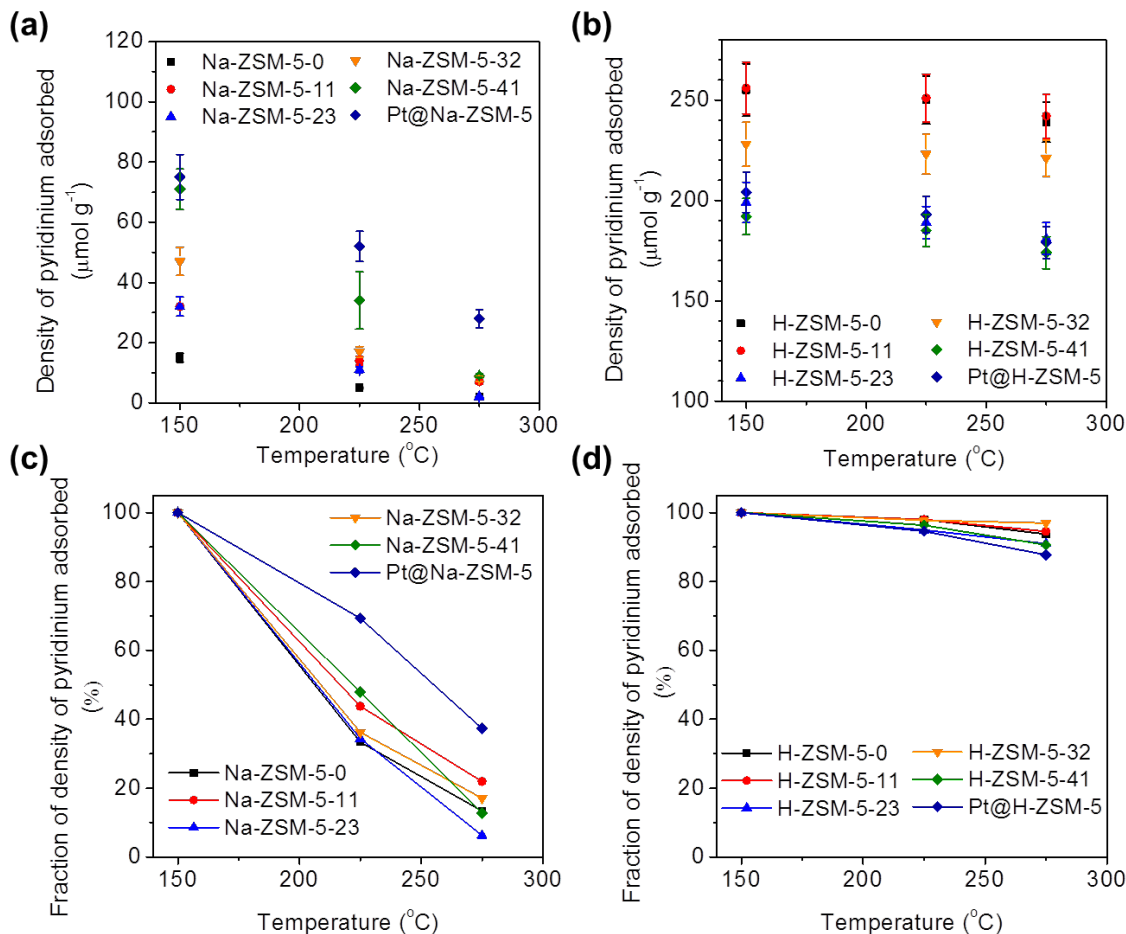


Figure S7. Amount of pyridinium adsorbed on (a) Na-ZSM-5-*X* samples and Pt@Na-ZSM-5, and (b) H-ZSM-5-*X* samples and Pt@H-ZSM-5, at different temperatures, and (c,d) temperature-programmed desorption (TPD) plots, respectively, on the basis of normalization with adsorbed pyridinium amount at 150 $^{\circ}\text{C}$.

Note: Acid characters of the materials could be estimated by TPD behaviors of pyridinium from BAS, as shown in Figure S7c and d. Compared with H-form samples, Na-form samples exhibits higher amount of pyridinium desorbed from BAS at lower temperature, suggesting different characters between BAS in intracrystalline mesopores and in micropores. One possibility is that the desorption of pyridinium (molecular size; 0.59 nm) from the BAS is enhanced in more spacious intracrystalline mesopores than in micropore channels (0.56 nm).¹¹ Another possible contributing factor is that the surrounding structures of BAS on the mesopores are not as crystalline as those in micropores, leading to the weaker acidity.

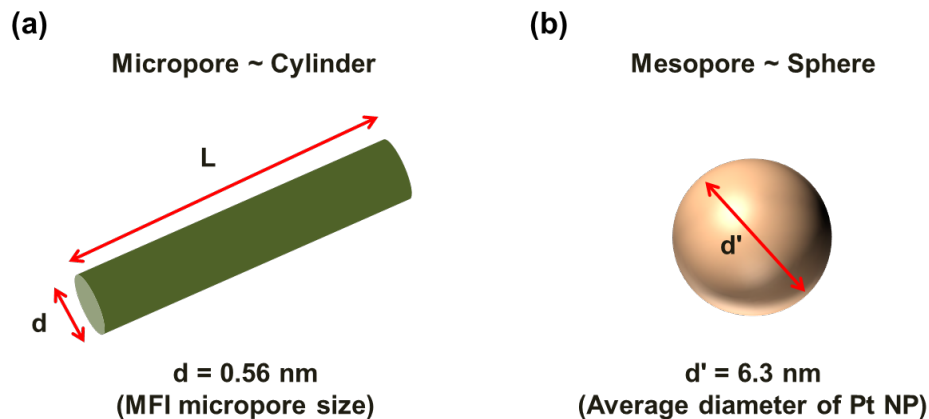


Figure S8. Estimation of surface area per unit pore volume for (a) micropore and (b) intracrystalline mesopore. Micropore and intracrystalline mesopore are simplified as cylindrical pore and spherical pore, respectively. Intracrystalline mesopore is assumed to be average Pt NP size determined by CO chemisorption.

Note:

$$\begin{aligned} \text{Ratio of surface area per pore volume} &= \frac{\frac{\text{Surface area of micropore}}{\text{Pore volume of micropore}}}{\frac{\text{Surface area of intracrystalline mesopore}}{\text{Pore volume of intracrystalline mesopore}}} \sim \frac{\frac{\pi d L}{\pi d^2 L / 4}}{\frac{4\pi (d'/2)^2}{4\pi (d'/2)^3 / 3}} \\ &= 7.5 \end{aligned}$$

This value means that micropore surface area is 7.5 times higher than intracrystalline mesopore volume per unit pore volume. Thus, the fraction of surface area of intracrystalline mesopore with respect to the sum of intracrystalline surface area and micropore surface area is $1/(1+7.5)$.

BAS density around intracrystalline mesopore with respective surface areas

$$= \text{BAS density around intracrystalline mesopore with respective pore volumes} \times \frac{1 + 7.5}{1} = 1.6 \times 8.5 = \mathbf{13.6}$$

The factor of 13.6 suggests that the BAS density is 13.6 times more enriched around intracrystalline mesopore than micropore surface, on the basis of pore surface area.

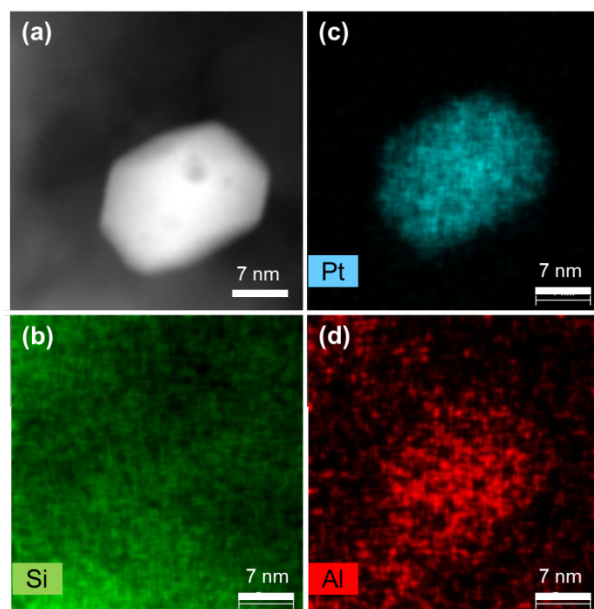


Figure S9. (a) a STEM image of Pt@H-ZSM-5, and (b-d) the elemental mapping of Si, Pt and Al of the same area around the Pt NP, respectively.

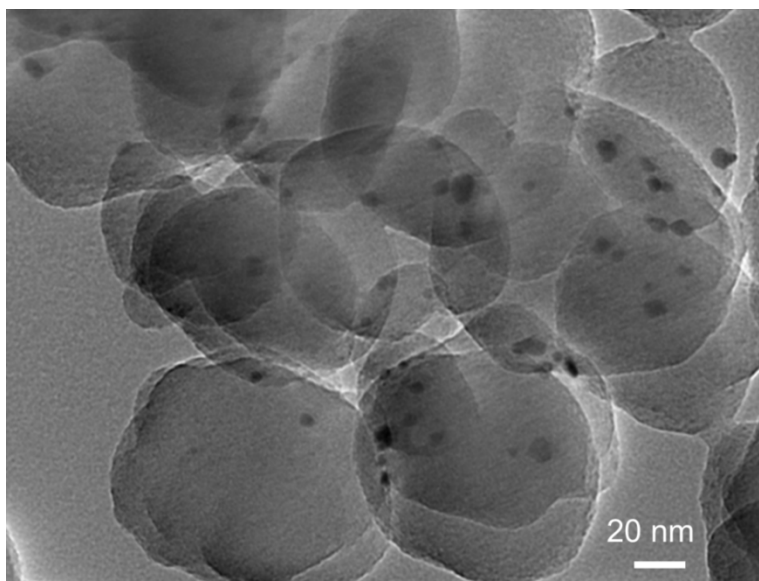


Figure S10. A TEM image of Pt/H-ZSM-5-0.

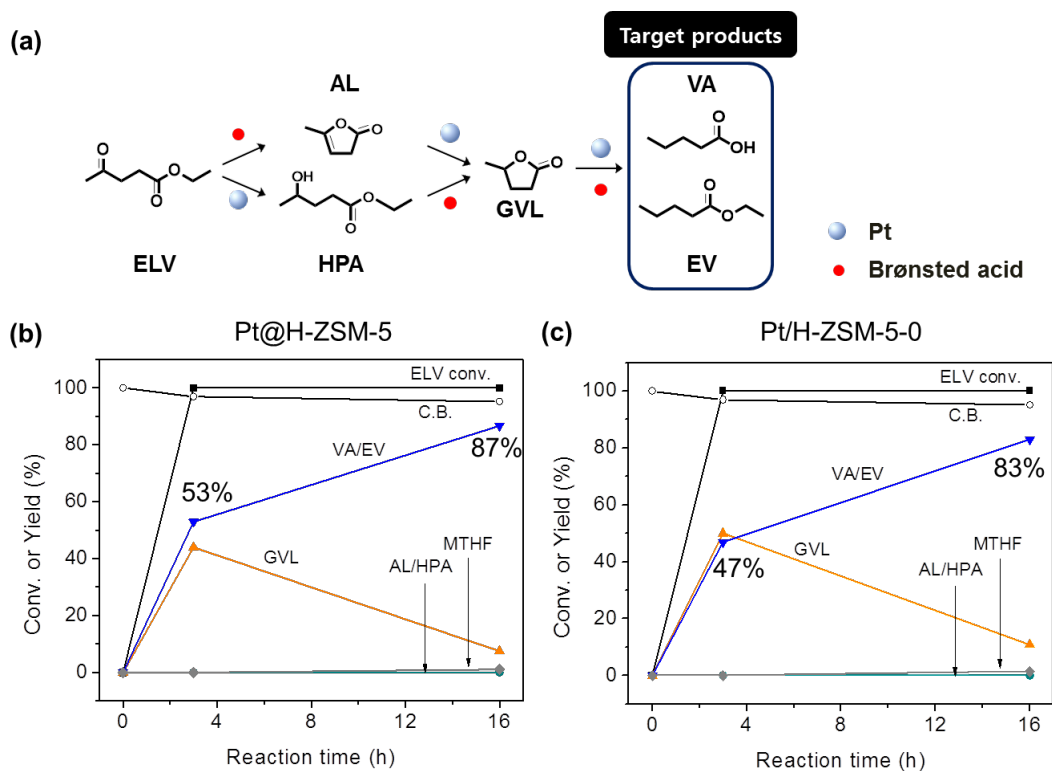


Figure S11. (a) Reaction network of conversion of ELV, and (b,c) time evolution of furfural conversion and product yields on of (b) Pt@H-ZSM-5 and (c) Pt/H-ZSM-5-0 in the ELV conversion into VA/EV performed at 140 °C.

Reaction conditions are as follows: 0.5 mmol of ELV, 4.5 mmol of EtOH and 1.5 mL of cyclohexane; 600 psi H₂; ELV/Al (mol mol⁻¹) = 24; ELV/Pt (mol mol⁻¹) = 616. Compounds involved in the reaction are denoted as follows: ethyl levulinate (ELV); γ -valerolactone (GVL); angelica lactone (AL); 4-hydroxy-pentanoic acid (HPA); valeric acid (VA); ethyl valerate (EV); 2-methyltetrahydrofuran (MTHF). The same abbreviations are used throughout this work.

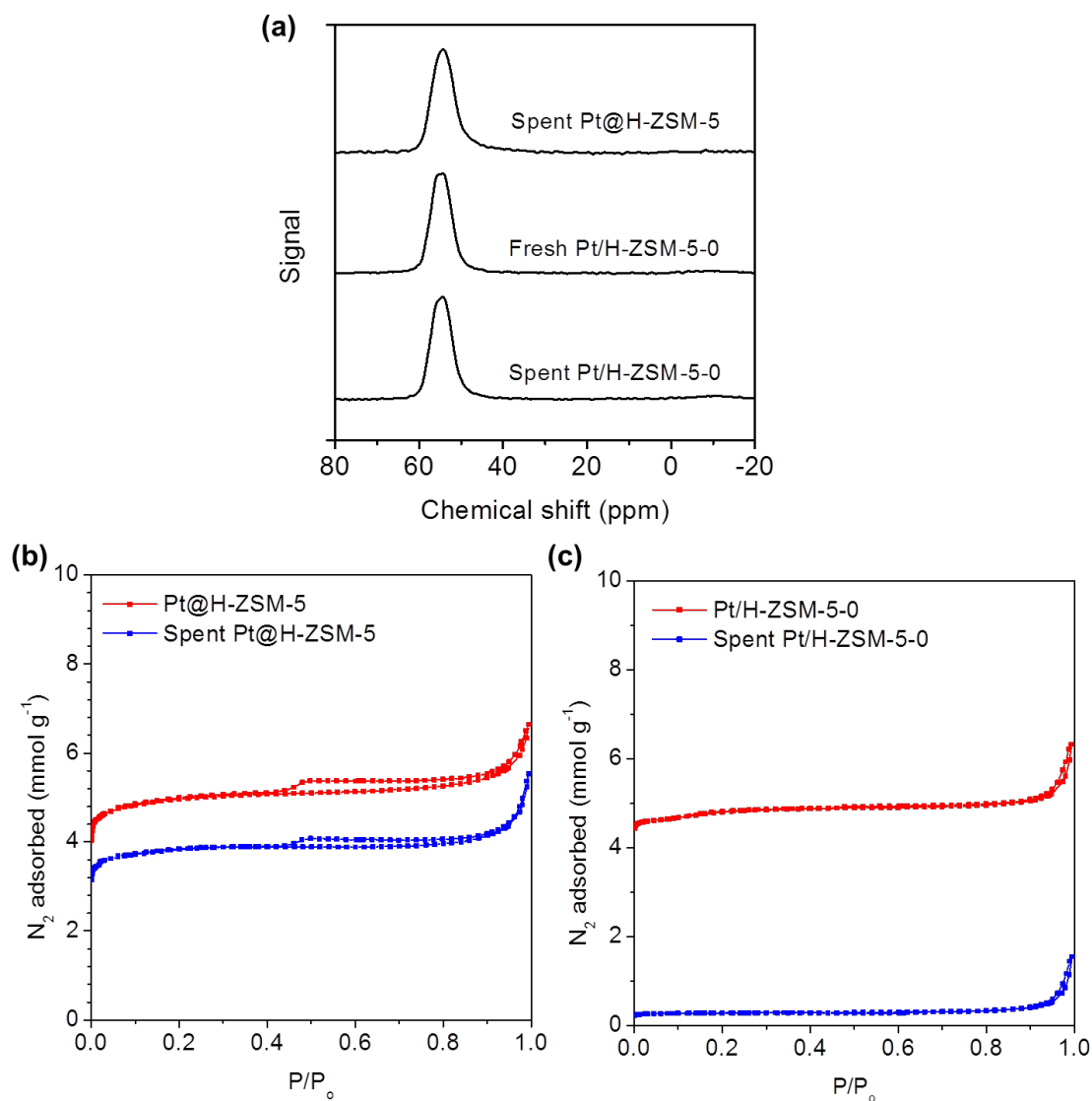


Figure S12. (a) ^{27}Al MAS NMR and (b,c) N_2 physisorption isotherms of the fresh and spent catalysts of Pt@H-ZSM-5 and Pt/H-ZSM-5-0. After 3 h of furfural reaction into VA/EV at 140 °C, the spent catalysts are collected, followed by washing with acetone and drying at 80 °C overnight prior to N_2 physisorption.

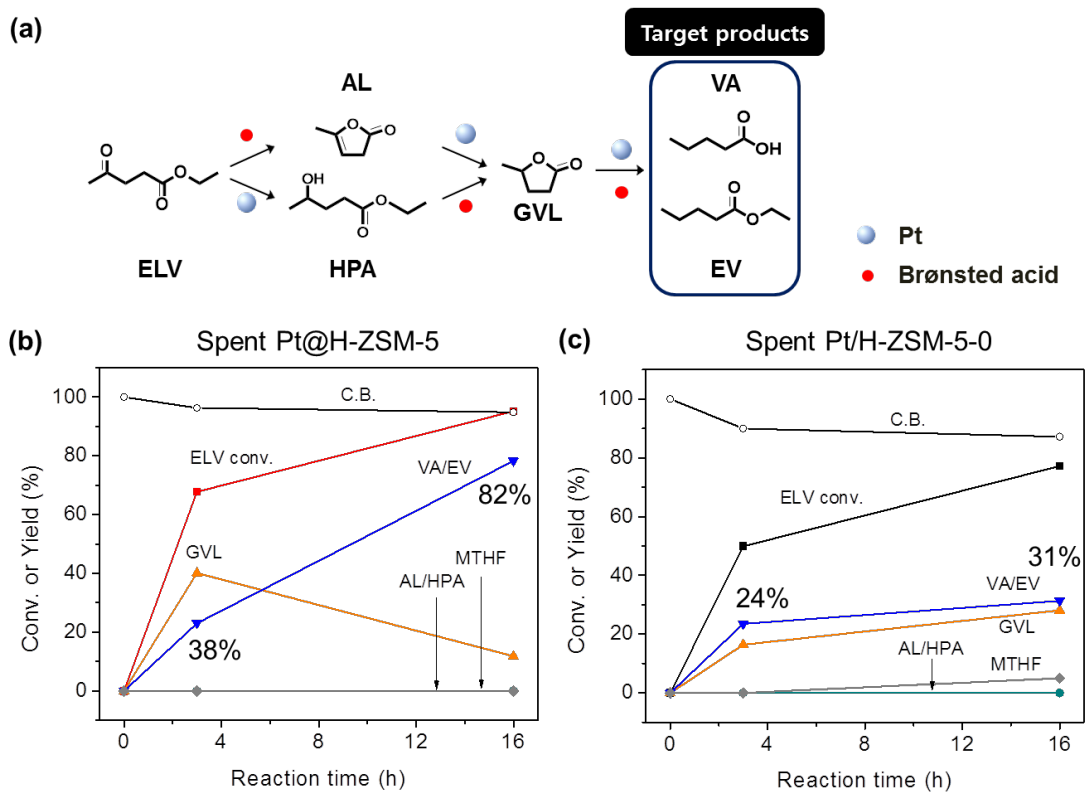


Figure S13. (a) Reaction network of conversion of ELV, and (b,c) time evolution of furfural conversion and product yields on (b) the spent Pt@H-ZSM-5 and (c) the spent Pt/H-ZSM-5-0 in the reaction starting with ELV at 140 °C.

Reaction conditions: 0.5 mmol of ELV, 4.5 mmol of EtOH and 1.5 mL of cyclohexane; 600 psi H₂; ELV/Al (mol mol⁻¹) = 24; ELV/Pt (mol mol⁻¹) = 616.

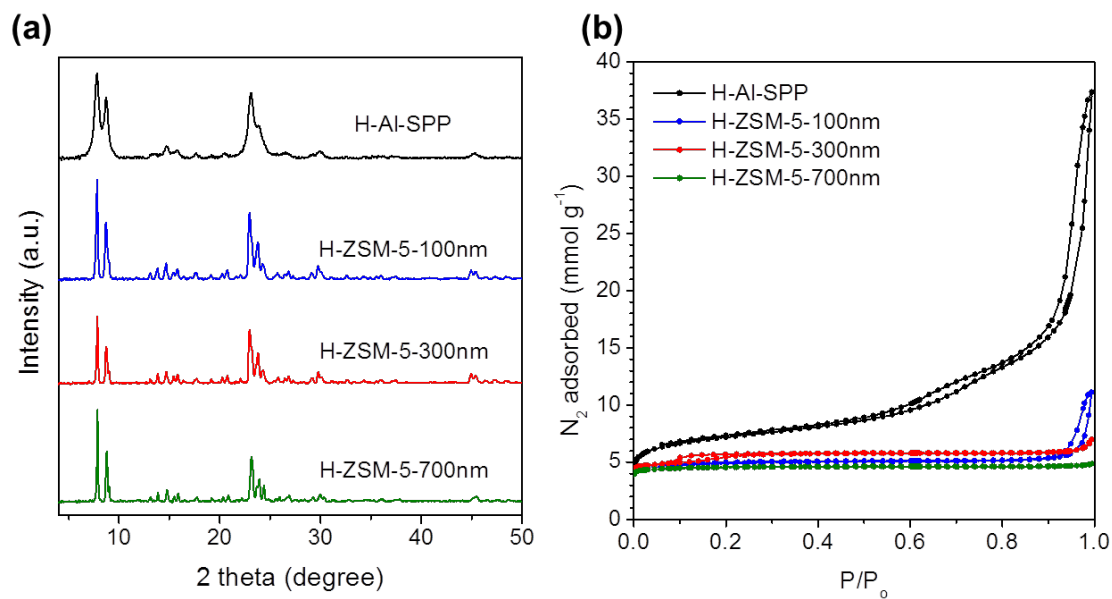


Figure S14. (a) XRD patterns and (b) N₂ physisorption isotherms of H-Al-SPP and H-ZSM-5-*Y* samples where *Y* refers to the average crystalline sizes of the MFI samples.

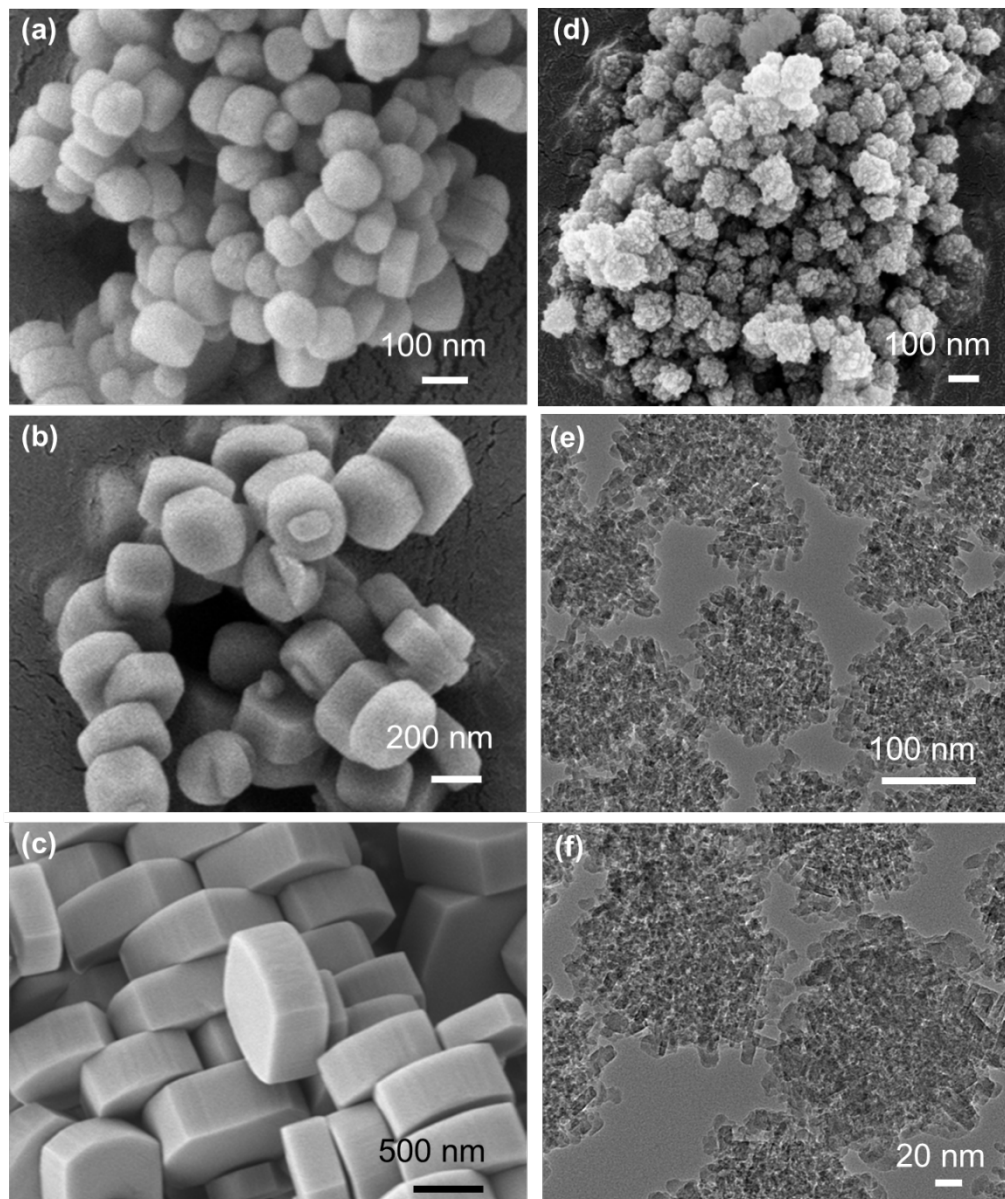


Figure S15. SEM images of (a) H-ZSM-5-100nm, (b) H-ZSM-5-300nm and (c) H-ZSM-5-700nm and (d) H-Al-SPP, and (e,f) TEM images of H-Al-SPP.

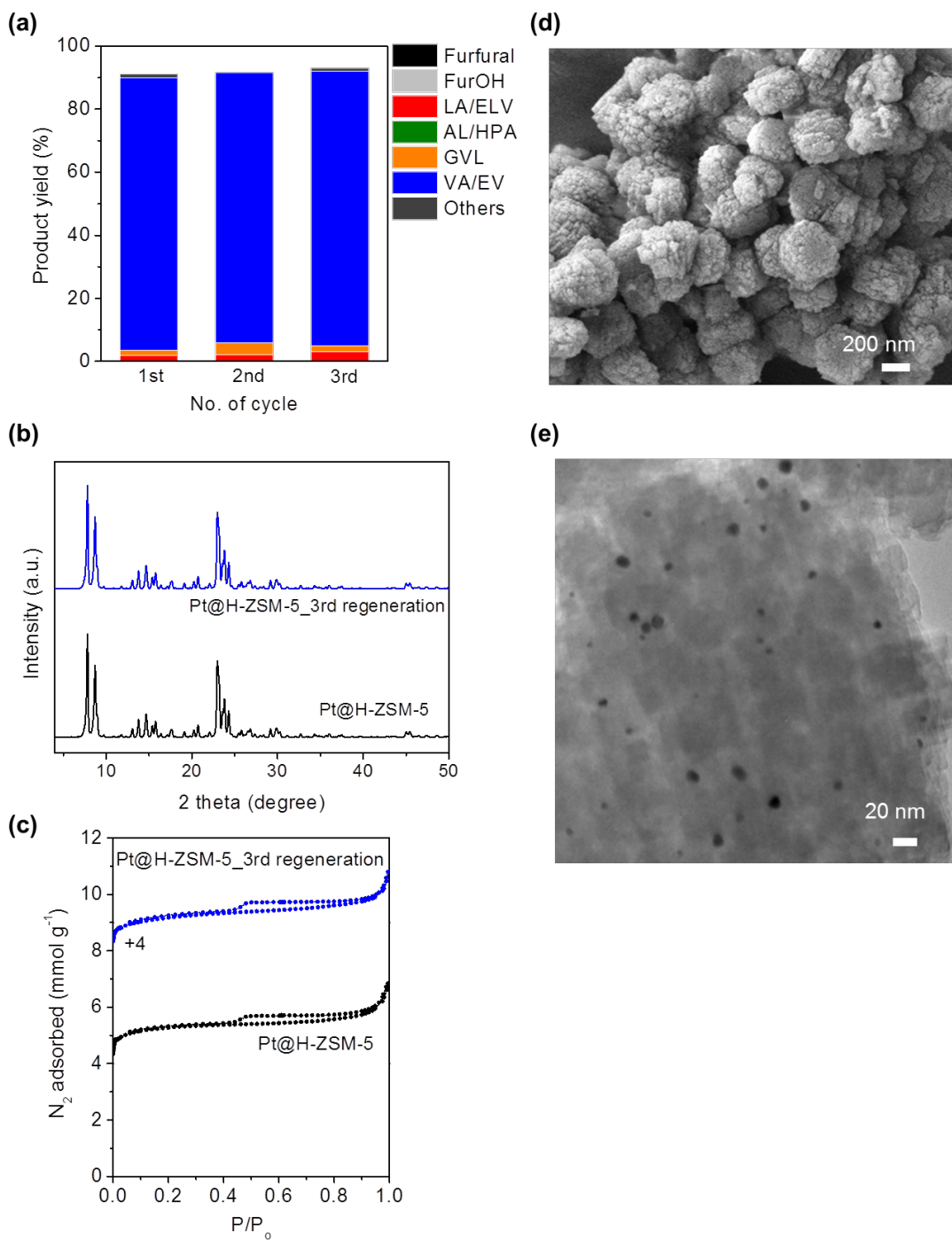


Figure S16. (a) Recyclability of Pt@H-ZSM-5, (b) XRD pattern, (c) N₂ physisorption isotherm, (d) SEM image and (e) TEM image of Pt@H-ZSM-5 after 3rd regeneration.

Table S1. Catalytic Results for Size-selective Oxidation of Cy6-ol and Cy12-ol^a

Catalyst	TOF (h ⁻¹) for Cy6-ol oxidation	TOF (h ⁻¹) for Cy12-ol oxidation	X^b	Y^c	Z^d
Pt@H-ZSM-5	32.4	1.1	29.5	11.8	0.92
Pt/H-ZSM-5-0	31.6	12.2	2.59	1.04	0.04
Pt/SiO ₂	36.2	14.5	2.50	-	-

^aReaction conditions are as follows: 0.1 mmol of Cy6-ol or Cy12-ol; 0.3 mmol TBHP; 2 mL acetonitrile; 60 °C.

$$^bX_{\text{sample}} = \text{TOF}_{\text{Cy6-ol}} / \text{TOF}_{\text{Cy12-ol}}.$$

$$^cY_{\text{sample}} = X_{\text{sample}} / X_{\text{Pt/SiO}_2}.$$

$$^dZ_{\text{sample}} = 1 - 1/Y_{\text{sample}}.$$

Table S2. Physical and Chemical Properties of the H-ZSM-5-*X* and Pt@H-ZSM-5 Samples

Catalyst	Nominal Si/Al (mol mol ⁻¹)	Si/Al ^a (mol mol ⁻¹)	BAS density ^b (μmol g ⁻¹)	Micropore volume ^c (cm ³ g ⁻¹)	Mesopore volume ^d (cm ³ g ⁻¹)
Na-ZSM-5-0	-	-	15	-	-
Na-ZSM-5-11	-	-	32	-	-
Na-ZSM-5-23	-	-	32	-	-
Na-ZSM-5-32	-	-	47	-	-
Na-ZSM-5-41	-	-	71	-	-
Pt@Na-ZSM-5	-	-	75	-	-
H-ZSM-5-0	60	46	255	0.15	0.0350
H-ZSM-5-11	60	49	237	0.14	0.0434
H-ZSM-5-23	60	54	208	0.15	0.0480
H-ZSM-5-32	60	52	229	0.14	0.0510
H-ZSM-5-41	60	57	192	0.14	0.0590
Pt@H-ZSM-5	60	57	204	0.14	0.0600

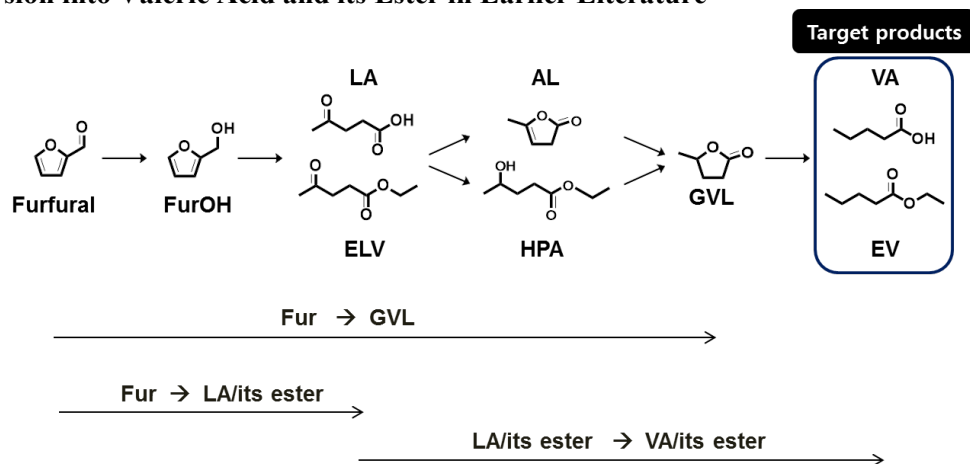
^aDetermined by XRF.

^bDetermined by quantitative FTIR spectroscopy with pyridine as the probe molecule at 150°C.

^cCalculated with the *t*-plot method obtained from N₂ physisorption isotherms.

^dDetermined by the BJH method (adsorption branch) obtained from N₂ physisorption isotherms.

Table S3. Catalyst Performances for Tandem Reactions Associated with Furfural Conversion into Valeric Acid and its Ester in Earlier Literature



Tandem reaction	Catalyst	Reaction conditions	Target products ^e	Ref.
Fur to VA/EV ^a	Pt@H-ZSM-5	140°C, 24h	VA/EV (86%)	This work
Fur to GVL ^b	Zr-BEA + Al-MFI-nanosheet	120°C, 48h	GVL (80%)	Bui et al. ¹²
	Au/ZrO ₂ + ZSM-5	120°C, 30h	GVL (80%)	Zhu et al. ¹³
	ZrO ₂ -SBA-15	170°C, 7h	GVL (35%)	Iglesias et al. ¹⁴
	Mesoporous Zr-Al-BEA	120°C, 24h	GVL (90%)	Song et al. ¹⁵
	Heteropoly acid/Zr-BEA	160°C, 24h	GVL (68%)	Winoto et al. ¹⁶
Fur to LA/its ester ^c	Au-H ₄ SiW ₁₂ O ₄₀ /ZrO ₂	120°C, 24h	LA/its ester (80%)	Zhu et al. ¹⁷
	Amberlyst 70	160°C, 2h	LA/its ester (47%)	Hu et al. ¹⁸
	Pt/ZrNbPO ₄	130°C, 6h	LA/its ester (70%)	Chen et al. ¹⁹
	Zr-SBA-15	260°C, 12h	LA/its ester (35%)	Chen et al. ²⁰
	Zr-MCM-41 + Amberlyst-15	130°C, 24h	LA/its ester (85%)	Peng et al. ²¹
LA/its ester to VA/its ester ^d	Ru/H-ZSM-5	200°C	VA/its ester (91%)	Luo et al. ²²
	Ru/H-ZSM-5	200°C	VA/its ester (99%)	Luo et al. ²³
	Ru/SBA-SO ₃ H	250°C, 6h	VA/its ester (94%)	Pan et al. ²⁴
	Co@H-ZSM-5	250°C	VA/its ester (90%)	Sun et al. ²⁵
	Pt/H-MFI	200°C, 1h	VA/its ester (78%)	Kon et al. ²⁶
	Ni/K0.5/H-ZSM-5	250°C	VA/its ester (90%)	Sun et al. ²⁷
	ZSM-5@(Co/SiO ₂)	250°C	VA/its ester (88%)	Wang et al. ²⁸
	Ni-W/H-ZSM-5	270°C	VA/its ester (26%)	Velisoju et al. ²⁹

^aConversion of furfural to VA/EV.

^bConversion of furfural to GVL.

^cConversion of furfural to LA and its ester.

^dConversion of LA and its ester to LA and its ester.

^eYields of target products in parenthesis.

Table S4. Physical and Chemical Properties of the Supported Pt Catalysts

Catalyst	Si/Al ^a (mol mol ⁻¹)	Pt ^a (wt%)	Micropore volume ^b (cm ³ g ⁻¹)
Pt/H-ZSM-5-0	46	0.26	0.15
Pt/H-ZSM-5-41	57	0.22	0.14
Pt/H-ZSM-5-100nm	62	0.22	0.13
Pt/H-ZSM-5-300nm	56	0.22	0.13
Pt/H-ZSM-5-700nm	58	0.22	0.14
Pt/H-Al-SPP	60	0.22	0.13
Pt/SiO ₂	-	0.80	0.00

^aDetermined by XRF.^bCalculated with the *t*-plot method obtained from N₂ physisorption isotherms.**Table S5. Physical and Chemical Properties of the Fresh and Spent Catalysts of Pt@H-ZSM-5 and Pt/H-ZSM-5-0**

Catalyst	Si/Al ^a (mol mol ⁻¹)	Pt ^a (wt%)	Micropore volume ^b (cm ³ g ⁻¹)
Pt@H-ZSM-5	57	0.22	0.14
Spent Pt@H-ZSM-5	57	0.22	0.11
Pt/H-ZSM-5-0	46	0.26	0.15
Spent Pt/H-ZSM-5-0	46	0.25	0.01

^aDetermined by XRF.^bCalculated with the *t*-plot method obtained from N₂ physisorption isotherms.**Table S6. Physical and Chemical properties of Pt@H-ZSM-5 after 3rd Regeneration**

Catalyst	Si/Al ^a (mol mol ⁻¹)	Pt ^a (wt%)	Micropore volume ^b (cm ³ g ⁻¹)	Pt size by CO chemisorption (nm)
Pt@H-ZSM-5	57	0.22	0.14	6.3
Pt@H-ZSM-5_3 rd regenerated	57	0.22	0.14	6.2

^aDetermined by XRF.^bCalculated with the *t*-plot method obtained from N₂ physisorption isotherms.

Table S7. Catalytic Results for Size-selective Oxidation of Cy6-ol and Cy12-ol with Regenerated Catalysts^a

Catalyst	TOF (h ⁻¹)	TOF (h ⁻¹)	X^b	Y^c	Z^d
	for Cy6-ol oxidation	for Cy12-ol oxidation			
Pt@H-ZSM-5	32.4	1.1	29.5	11.8	0.92
Pt@H-ZSM-5_3 rd regenerated	32.5	1.2	27.1	10.8	0.91
Pt/SiO ₂	36.2	14.5	2.50	-	-

^aReaction conditions are as follows: 0.1 mmol of Cy6-ol or Cy12-ol; 0.3 mmol TBHP; 2 mL acetonitrile; 60 °C.

^b $X_{\text{sample}} = \text{TOF}_{\text{Cy6-ol}} / \text{TOF}_{\text{Cy12-ol}}$.

^c $Y_{\text{sample}} = X_{\text{sample}} / X_{\text{Pt/SiO}_2}$.

^d $Z_{\text{sample}} = 1 - 1/Y_{\text{sample}}$.

References

- (1) Mochizuki, H.; Yokoi, T.; Imai, H.; Watanabe, R.; Namba, S.; Kondo, J. N.; Tatsumi, T. Facile control of crystallite size of ZSM-5 catalyst for cracking of hexane. *Micropor. Mesopor. Mat.* **2011**, *145*, 165-171.
- (2) Zhang, X. Y.; Liu, D. X.; Xu, D. D.; Asahina, S.; Cychosz, K. A.; Agrawal, K. V.; Al Wahedi, Y.; Bhan, A.; Al Hashimi, S.; Terasaki, O.; Thommes, M.; Tsapatsis, M. Synthesis of Self-Pillared Zeolite Nanosheets by Repetitive Branching. *Science* **2012**, *336*, 1684-1687.
- (3) Cho, H. J.; Kim, D.; Li, J.; Su, D.; Xu, B. J. Zeolite-Encapsulated Pt Nanoparticles for Tandem Catalysis. *J. Am. Chem. Soc.* **2018**, *140*, 13514-13520.
- (4) Goel, S.; Zones, S. I.; Iglesia, E. Encapsulation of Metal Clusters within MFI via Interzeolite Transformations and Direct Hydrothermal Syntheses and Catalytic Consequences of Their Confinement. *J. Am. Chem. Soc.* **2014**, *136*, 15280-15290.
- (5) Thommes, M.; Cychosz, K. A. Physical adsorption characterization of nanoporous materials: progress and challenges. *Adsorption* **2014**, *20*, 233-250.
- (6) Gamliel, D. P.; Cho, H. J.; Fan, W.; Valla, J. A. On the effectiveness of tailored mesoporous MFI zeolites for biomass catalytic fast pyrolysis. *Appl. Catal. A* **2016**, *522*, 109-119.
- (7) Yoo, W. C.; Zhang, X. Y.; Tsapatsis, M.; Stein, A. Synthesis of mesoporous ZSM-5 zeolites through desilication and re-assembly processes. *Micropor. Mesopor. Mater.* **2012**, *149*, 147-157.
- (8) Paixao, V.; Carvalho, A. P.; Rocha, J.; Fernandes, A.; Martins, A. Modification of MOR by desilication treatments: Structural, textural and acidic characterization. *Micropor. Mesopor. Mat.* **2010**, *131*, 350-357.
- (9) Yokoi, T.; Mochizuki, H.; Namba, S.; Kondo, J. N.; Tatsumi, T. Control of the Al Distribution in the Framework of ZSM-5 Zeolite and Its Evaluation by Solid-State NMR Technique and Catalytic Properties. *J. Phys. Chem. C* **2015**, *119*, 15303-15315.
- (10) Jacobsen, C. J. H.; Madsen, C.; Janssens, T. V. W.; Jakobsen, H. J.; Skibsted, J. Zeolites by confined space synthesis - characterization of the acid sites in nanosized ZSM-5 by ammonia desorption and Al-27/Si-29-MAS NMR spectroscopy. *Micropor. Mesopor. Mat.* **2000**, *39*, 393-401.
- (11) Borade, R. B.; Adnot, A.; Kaliaguine, S. Acid Sites in Dehydroxylated Y Zeolites - an X-Ray Photoelectron and Infrared Spectroscopic Study Using Pyridine as a Probe Molecule. *J. Chem. Soc. Faraday Trans.* **1990**, *86*, 3949-3956.
- (12) Bui, L.; Luo, H.; Gunther, W. R.; Roman-Leshkov, Y. Domino Reaction Catalyzed by Zeolites with Brønsted and Lewis Acid Sites for the Production of γ -Valerolactone from Furfural. *Angew. Chem. Int. Ed.* **2013**, *52*, 8022-8025.
- (13) Zhu, S. H.; Xue, Y. F.; Guo, J.; Cen, Y. L.; Wang, J. G.; Fan, W. B. Integrated Conversion of Hemicellulose and Furfural into γ -Valerolactone over Au/ZrO₂ Catalyst Combined with ZSM-5. *ACS Catal.* **2016**, *6*, 2035-2042.
- (14) Iglesias, J.; Melero, J. A.; Morales, G.; Paniagua, M.; Hernandez, B.; Osatiashtiani, A.; Lee, A. F.; Wilson, K. ZrO₂-SBA-15 catalysts for the one-pot cascade synthesis of GVL from furfural. *Catal. Sci. Technol.* **2018**, *8*, 4485-4493.
- (15) Song, S.; Di, L.; Wu, G. J.; Dai, W. L.; Guan, N. J.; Li, L. D. Meso-Zr-Al-beta zeolite as a robust catalyst for cascade reactions in biomass valorization. *Appl. Catal. B* **2017**, *205*, 393-403.
- (16) Winoto, H. P.; Fikri, Z. A.; Ha, J. M.; Park, Y. K.; Lee, H.; Suh, D. J.; Jae, J. Heteropolyacid supported on Zr-Beta zeolite as an active catalyst for one-pot transformation of furfural to γ -valerolactone. *Appl. Catal. B* **2019**, *241*, 588-597.

- (17) Zhu, S. H.; Cen, Y. L.; Guo, J.; Chai, J. C.; Wang, J. G.; Fan, W. B. One-pot conversion of furfural to alkyl levulinate over bifunctional Au-H₄SiW₁₂O₄₀/ZrO₂ without external H₂. *Green Chem.* **2016**, *18*, 5667-5675.
- (18) Hu, X.; Jiang, S. J.; Wu, L. P.; Wang, S.; Li, C. Z. One-pot conversion of biomass-derived xylose and furfural into levulinate esters via acid catalysis. *Chem. Commun.* **2017**, *53*, 2938-2941.
- (19) Chen, B. F.; Li, F. B.; Huang, Z. J.; Lu, T.; Yuan, Y.; Yuan, G. Q. Integrated Catalytic Process to Directly Convert Furfural to Levulinate Ester with High Selectivity. *ChemSusChem* **2014**, *7*, 202-209.
- (20) Chen, H.; Ruan, H. H.; Lu, X. L.; Fu, J.; Langrish, T.; Lu, X. Y. Catalytic conversion of furfural to methyl levulinate in a single-step route over Zr/SBA-15 in near-critical methanol. *Chem. Eng. J* **2018**, *333*, 434-442.
- (21) Peng, L. C.; Gao, X. Y.; Yu, X.; Li, H.; Zhang, J. H.; He, L. Facile and High-Yield Synthesis of Alkyl Levulinate Directly from Furfural by Combining Zr-MCM-41 and Amberlyst-15 without External H₂. *Energy Fuels* **2019**, *33*, 330-339.
- (22) Luo, W. H.; Deka, U.; Beale, A. M.; van Eck, E. R. H.; Bruijninx, P. C. A.; Weckhuysen, B. M. Ruthenium-catalyzed hydrogenation of levulinic acid: Influence of the support and solvent on catalyst selectivity and stability. *J. Catal.* **2013**, *301*, 175-186.
- (23) Luo, W. H.; Bruijninx, P. C. A.; Weckhuysen, B. M. Selective, one-pot catalytic conversion of levulinic acid to pentanoic acid over Ru/H-ZSM5. *J. Catal.* **2014**, *320*, 33-41.
- (24) Pan, T.; Deng, J.; Xu, Q.; Xu, Y.; Guo, Q. X.; Fu, Y. Catalytic conversion of biomass-derived levulinic acid to valerate esters as oxygenated fuels using supported ruthenium catalysts. *Green Chem.* **2013**, *15*, 2967-2974.
- (25) Sun, P.; Gao, G.; Zhao, Z. L.; Xia, C. G.; Li, F. W. Stabilization of Cobalt Catalysts by Embedment for Efficient Production of Valeric Biofuel. *ACS Catal.* **2014**, *4*, 4136-4142.
- (26) Kon, K.; Onodera, W.; Shimizu, K. Selective hydrogenation of levulinic acid to valeric acid and valeric biofuels by a Pt/HMFI catalyst. *Catal. Sci. Technol.* **2014**, *4*, 3227-3234.
- (27) Sun, P.; Gao, G.; Zhao, Z. L.; Xia, C. G.; Li, F. W. Acidity-regulation for enhancing the stability of Ni/HZSM-5 catalyst for valeric biofuel production. *Appl. Catal. B* **2016**, *189*, 19-25.
- (28) Wang, D. R.; Wang, B.; Ding, Y. Q.; Yuan, Q. Q.; Wu, H. H.; Guan, Y. J.; Wu, P. Robust synthesis of green fuels from biomass-derived ethyl esters over a hierarchically core/shell-structured ZSM-5@(Co/SiO₂)catalyst. *Chem. Commun.* **2017**, *53*, 10172-10175.
- (29) Velisoju, V. K.; Gutta, N.; Tardio, J.; Bhargava, S. K.; Vankudoth, K.; Chatla, A.; Medak, S.; Akula, V. Hydrodeoxygenation activity of W modified Ni/H-ZSM-5 catalyst for single step conversion of levulinic acid to pentanoic acid: An insight on the reaction mechanism and structure activity relationship. *Appl. Catal. A* **2018**, *550*, 142-150.